Glassy Dynamics in the Folding Landscape of Cytochrome *c* Detected by Laser Photolysis†

M. Yadaiah, Rajesh Kumar, and Abani K. Bhuyan*

School of Chemistry, University of Hyderabad, Hyderabad 500046, India

Received October 22, 2006; Revised Manuscript Received December 12, 2006

ABSTRACT: Ferrocytochrome *c* liganded with CO refolds to a nativelike compact state, called the M state, where the non-native Fe^{2+}−CO contact persists. The M state resembles the generic molten globule-like states and can be driven to the native state by pulsed laser photolysis of the CO ligand. The microsecond kinetics measured all across the guanidine hydrochloride unfolding transition of the protein produce a chevron plot with accentuated rollover in the folding limb, suggesting a glass transition of M en route to N. The rate of exit of the folding structure from the kinetic trap(s) limits the overall rate of folding of M to N. Sulfate-induced deceleration of the observed folding rate suggests that the folding structure indeed is transiently frozen in glassy traps. The results connect the post-transition features of the funnel paradigm.

The emergence of theoretical models inspired by the folding of lattice polymers (*1*−*10*) has fuelled the excitement in protein folding research very significantly. These studies have unraveled the complexity of the folding process within the framework of the sequence-based organization of conformational energies into a funnel landscape (*11*). Remarkably, the organization of the energy landscape appears to offer a variety of mechanisms for approaching the folding problem from thermodynamic, kinetic, evolutionary, and sequence-selection viewpoints (*9*). Such developments most definitely invite intense collaboration between theory and experiments. Several theoretical studies already appear to agree closely with experiments regarding the rate-limiting structures, folding intermediates, and speed limit of real proteins (*10*, *12*−*18*). Experimental studies, especially those engaging laser-based kinetic methods (*19*−*22*) and protein engineering approaches (*23*, *24*), have also begun to reciprocate (*25*). A nice illustration of such studies is the recent demonstration of downhill (type 0) folding under native-biased conditions (*26*).

A basic finding of theory is that discrete kinetic intermediates appear very late in folding (*11*). Post-transition late intermediates that are structurally nativelike have been detected independently by native-state hydrogen exchange experiments using cytochrome *c* (*27*−*29*). Even though the modified classical pathway that fits these experimental data is conceptually different from the landscape funnel regarding at least the "barrier mechanism", both enumerate nativelike intermediates. Accordingly, even for an apparently two-state protein like cytochrome *c*, the energy landscape can be rough everywhere along the reaction coordinate, not just near the unfolded state.

Another fundamental element of the funneling process is that folding is dominated by glassy dynamics once the folding ensemble has passed from the compact molten globule-like band over the transition-state region of the funnel. Folding is blocked as long as the protein stays frozen in the kinetic traps, and a reorganization of the misconfigured interactions is required for descending to the native well (*7*, *11*). In the effort of connecting this prediction of the theory, experimental work has focused on the nature of the exponential relaxation during folding, since glass transitions are characterized by stretched exponentials (*30*). Earlier observations of the non-single-exponential nature of folding (*31*, *32*) appeared to indicate glassy dynamics. In more recent ultrafast experiments, helix formation kinetics has been found to be stretched exponential (*33*). On the other hand, single-exponential, and hence nonglassy, kinetics for the folding of protein L at low temperatures has also been reported (*34*). However, simple single-exponential kinetics can often produce rate rollover due to kinetic trapping and glassy dynamics (see below).

This work shows how a molten globule-like late intermediate enters glassy dynamics as the protein runs down the folding funnel. We have used ferrocytochrome *c*, the paradigmatic fast folding, two-state protein that preserves the folding speed even when the native Fe^{2+}−M80 link is replaced with a Fe^{2+}−CO link by using extrinsic CO ligand (*35*, *36*). In the stopped-flow experiment, the CO-liganded protein (carbonmonoxycyt *c*)[1] refolds rapidly with the Fe^{2+}−CO interaction intact. This natively folded species, labeled the M state, exhibits the generic properties of molten globule-like states and was first used in this laboratory to study the protein stiffening effect of subdenaturing concentrations of

† This work was supported by grants from the Department of Biotechnology (BRB/15/227/2001), the Department of Science and Technology (4/1/2003-SF), and the University Grants Commission (UPE Funding), Government of India. A.K.B. is the recipient of a Swarnajayanti Fellowship from the Department of Science and Technology.

* To whom correspondence should be addressed. E-mail: akbsc@uohyd.ernet.in. Phone: 91-40-2313-4810. Fax: 91-40-2301-2460.

[1] Abbreviations: GdnHCl, guanidinium chloride; cyt, cytochrome; ferrocyt, ferrocytochrome; cyt-CO, carbonmonoxide-liganded ferrocytochrome *c*; MG, molten globule.

10.1021/bi062193u CCC: $37.00
Published on Web 02/09/2007

denaturants (*37*, *38*). Pabit et al. (*39*) have elegantly subjected the M state to laser photolysis to investigate the role of internal friction in protein folding. Along the same line, we have employed a nanosecond laser pulse to photodissociate the CO ligand over the entire range of aqueous solubilities of guanidinium hydrochloride (GdnHCl). In the effort to establish the folding dynamics of the molten globule-like state, we treat the kinetic data as a chevron. Analyses indicate that the M → N folding proceeds via at least one glassy state that gives rise to rate rollover in the chevron plot. For simplicity, we liken this process to the phenomenological M → I → N folding, where the I state belongs to a set of trapped intermediates. Further, we show that the misorganized interactions in the I state must be reorganized to achieve the native state and that the energy barrier for the exit from the kinetic trap is fairly high. Overall, the paper highlights the connection between "classic" kinetic models and landscape models.

MATERIALS AND METHODS

Cyt *c* was from Sigma (type VI). Experiments were performed in a strictly anaerobic atmosphere, at 22 °C, in 0.1 M sodium phosphate buffer (pH 7) containing 0.5−3 mM freshly prepared sodium dithionite. The concentration of GdnHCl was determined by refractive indices.

Equilibrium Unfolding. Samples of cytochrome *c* (10−15 μM protein) were prepared in the range of 0−7 M GdnHCl. The solutions were deaerated and reduced under nitrogen with 0.5−1 mM sodium dithionite. The samples were saturated with CO by passing a slow stream of the dry gas into the solutions for 1 min. The tubes were then capped with sleeved rubber stoppers and incubated for ~45 min. The tryptophan fluorescence excited at 280 nm was measured at 358 nm using a photon counting instrument.

Preparation of the M State (*the CO-liganded nativelike ferrocytochrome c*). Cytochrome *c* (0.6 mM), initially dissolved in 6.35 M GdnHCl and 0.1 M phosphate (pH 7), was deaerated, reduced, and liganded with CO. Ferrocyt *c* thus obtained (called UCO) is completely unfolded. UCO was then diluted at least 20-fold by transferring a required volume of the solution into a cuvette containing 2 mL of the degassed and dithionite-reduced CO-free refolding buffer [0.1 M phosphate (pH 7) at 22 °C containing the desired solvent additive]. This procedure allows complete refolding of ferrocyt *c* to the M state. The M-state preparation was used up as quickly as possible, usually within 5 min.

Stopped-Flow Kinetics of the UCO ⇌ M Reaction. Cytochrome *c* (318 μM), initially unfolded in 6.35 M GdnHCl (pH 7) and reduced under nitrogen with 3.2 mM sodium dithionite, was reacted with CO. The CO-saturated unfolded protein solution contained in a gastight syringe was mounted on the stopped-flow mixing module and equilibrated at 22 °C for ~20 min. Similarly, the dithionite-reduced refolding buffer that did not contain CO was also mounted and equilibrated at the same temperature. Folding was initiated by two-syringe mixing (1:7 protein:buffer ratio) with a total flow rate of 8 mL/s. This procedure ensures minimal air oxidation of the protein. The final protein concentration in the refolding mixture was 39 μM.

The same procedure was used for unfolding experiments. The M state was prepared by 45-fold dilution of the UCO solution following the procedure described above. The final protein concentration was ~3 μM. A Bio-Logic SFM 400 instrument was used.

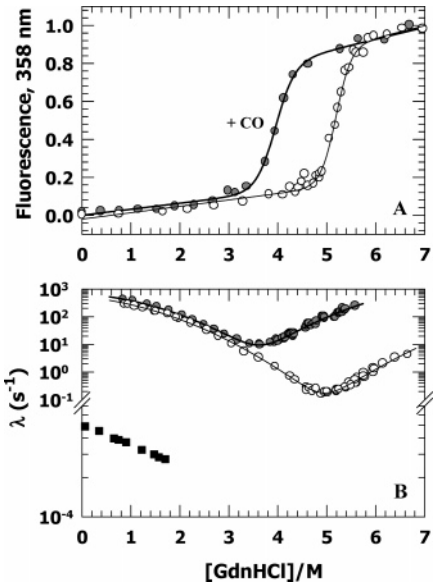

FIGURE 1: (A) Equilibrium unfolding of ferrocyt *c* illustrating the mass action effect of CO. Values of $\Delta G°$ (kilocalories per mole) and m_g (kilocalories per mole per molar) obtained from standard two-state analysis are 11 ± 1 and 2.95 ± 0.2 in the presence of CO and 19 ± 0.5 and 3.6 ± 0.2 in the absence of CO, respectively. (B) Effect of the Fe^{2+}−CO interaction on the millisecond folding chevron. In the presence of CO, the chevron is shifted both horizontally and vertically. The refolding rate is only marginally affected. To account for curvatures in the chevron limb, the data were fitted assuming a quadratic dependence of rates on the denaturant. Also shown is the denaturant dependence of the rate of thermal dissociation of CO from the NCO or M state (■).

Laser Photolysis and Microsecond Kinetics of the M → N Reaction. The M-state preparation contained in a tightly capped quartz cuvette was equilibrated for 3 min at the desired temperature in the spectrometer cuvette holder. CO photolysis was achieved by irradiation with 90 ± 10 mJ pulses of the 532 nm second-harmonic output of a Spectra Physics Q-switched Nd/YAG laser (10 Hz). Spectral changes at 550 nm following the photolysis pulse were recorded with a pulsed Xe lamp. Photolysis was nearly complete, since another laser shot pulsed immediately afterward produced insignificant spectral changes. A fresh sample was used for each single-pulse kinetic trace. For each concentration of GdnHCl, four or five kinetic traces were taken. The basic configuration of the instrument is based on the Applied Photophysics laser-flash photolysis spectrometer. The temperature of the cuvette holder was maintained by using an external circulating water bath.

RESULTS AND DISCUSSION

Routing Ferrocytochrome c to a Molten Globule-like M State. The Fe^{2+}−M80 covalent link of ferrocyt *c*, which is very stable under physiological conditions, weakens when the protein is destabilized, thereby allowing the binding of exogenous ligands such as CO and NO to the heme iron. Figure 1a illustrates the effect of preferential binding of CO to the unfolded state on the GdnHCl-induced transition of ferrocyt *c* at 22 °C. CO binds tightly to the unfolded protein

($K_a \sim 21\ \mu M^{-1}$) and lowers the folding free energy by ~8.1 kcal/mol.

When the unfolded protein solution liganded with CO (UCO) is diluted into a refolding medium, the protein collapses and forms a nativelike "intermediate" state (NCO or M) in which the $Fe^{2+}-CO$ interaction persists for a considerably long time. The NCO state can also be driven to unfold when the solution is transferred to the unfolding buffer. Figure 1b shows that the millisecond rates for the refolding of UCO are only marginally faster than those for the unfolded protein without CO (U). The unfolding rates of NCO are, however, much faster. Because the concentration of CO in the final refolding medium is substantially low and the $Fe^{2+}-M80$ interaction is preferred over the $Fe^{2+}-CO$ interaction, the trapped CO escapes as thermal motions facilitate the dissociation of the $Fe^{2+}-CO$ bond. The time constant for this thermal process (NCO → N + CO) measured by changes in optical absorbance at 550 nm is ~45 min (Figure 1b and refs *37* and *38*). The thermally activated CO dissociation limits the overall UCO → N refolding and thus renders the NCO → N part of the refolding reaction invisible. The NCO → N process can, however, be captured by recording the kinetics of conformational changes following photodissociation of CO.

The differences in kinetics of the UCO ⇌ NCO and U ⇌ N reactions suggest that NCO and N are energetically and structurally somewhat disparate. From simple thermodynamic calculations using the data shown in Figure 1a, and the comparison of spectral signatures of N and NCO, provided as Supporting Information, it can be shown that (i) NCO is less stable than N by ~2 kcal/mol (*35*) and (ii) it fairly fits into the molecular organizational definition of the classic molten globule (MG) state (*40*, *41*). The fluorescence and far-UV CD spectra of NCO are nearly identical to those for N. The near-UV CD absorption of NCO is, however, substantially weaker than that for N. Also, the ^1H NMR spectra of NCO and the alkali MG state of ferrocytochronme *c* match very closely (data provided as Supporting Information). These observations suggest that NCO represents a compact and largely mobile molecular state containing nativelike secondary structure and hydrodynamic radius, but without rigid tertiary structure. To emphasize such similarities of NCO and MG states, we call NCO the M state. Thus, the study reports on the reaction kinetics of the late molten globule-like M state (M → N) and relates the observed behavior to the predictions of the funnel paradigm.

M → N Kinetics Observed by Laser Photolysis. As mentioned above, the M → N process is difficult to study, because the folding kinetics are rate-limited by very slow thermal dissociation of the $Fe^{2+}-CO$ bond. In the photodissociation protocol, the CO dissociation occurs in the subpicosecond regime so that the slower relaxations associated with the dynamics of side chain folding can be conveniently monitored. Figure 2a shows the microsecond kinetics of the M → N transition in 0.85 M GdnHCl initiated by a single-pulse laser photolysis. The time evolution of the optical absorbance of N is adequately described by a single exponential with a rate constant (k_f) of $1.7 \times 10^5\ s^{-1}$ ($\tau = 5.9\ \mu s$). Rates measured at several concentrations of GdnHCl all across the unfolding transition of ferrocyt *c* are plotted in Figure 2b. Clearly, k_f rolls over in the pretransition region (<2.6 M GdnHCl) where ferrocyt *c* is most stable but

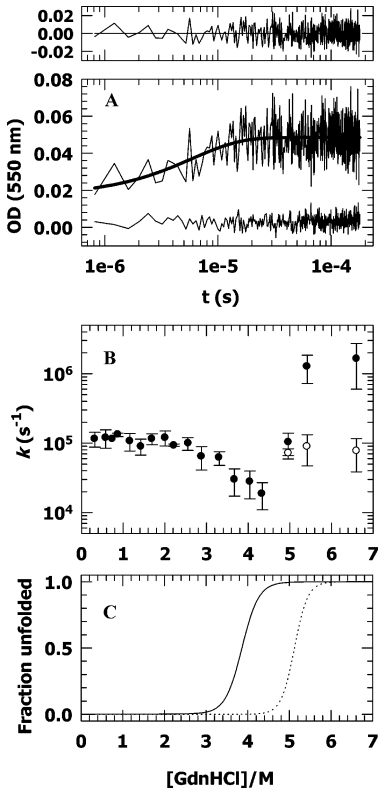

FIGURE 2: Microsecond kinetics for the folding of M. (A) Single-pulse laser photolysis of CO from the M state in the presence of 0.85 M GdnHCl. Subsequent laser shots produce no change in absorbance (bottom trace), indicating that the folded protein does not rebind CO under the conditions of low gas pressure and strongly refolding solvent. The residual in the top panel indicates that the relaxation is adequately monophasic ($k_f = 1.7 \times 10^5\ s^{-1}$; $\tau = 5.9\ \mu s$). (B) Chevron plot for the folding of the M state. As described in the text, the biphasic relaxations under the unfolding conditions (>4.5 M GdnHCl) correspond to ligand exchange dynamics reported previously (*39*−*41*). That the rates measured in <4.5 M GdnHCl correspond to refolding relaxations is consistent with the CO-induced shift in the unfolding transition of ferrocyt *c* (C).

decreases rapidly as progressively destabilizing conditions are employed. The decrease continues to the region where the CO-liganded protein is unfolded, but the unliganded protein is not. Passing this, the transition region of ferrocyt *c* is approached (>4.4 M GdnHCl) where the postphotolysis kinetics begins to accelerate in two distinct phases. These two phases are assigned to, in decreasing order of rate coefficient, transient bindings of methionines (M65 and M80) and histidines (H18 and H33) to the heme iron, consistent with earlier studies of postphotolysis chain dynamics (*19*, *42*−*44*). The biphasic relaxation following CO photolysis is the hallmark of heme−polypeptide dynamics in the unfolded state of ferrocyt *c*. Thus, the rates in the range of 0−4.4 M GdnHCl contain the information relevant to the M → N conformational transition. We note that the rate constant for this transition extracted by linear extrapolation of the rate data from the transition region to the ordinate is $\approx 1 \times 10^6\ s^{-1}$ for k°_{MI} ($\tau = 1\ \mu s$). This is the fastest achievable rate for the M → N transition in the absence of a trapped intermediate and is within the range set for limited structural events, including local hydrophobic collapse (*45*), and the folding of the model peptide α-helix (*46*−*48*) and β-hairpin fragment (*49*). It also closely matches the rate of

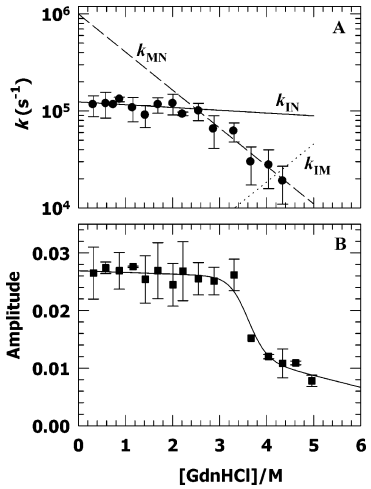

FIGURE 3: (A) Rate rollover in the folding limb can be explained on the basis of glassy dynamics. The exit of the frozen folding structures from kinetic traps limits the overall folding rate, giving rise to rate rollover. Within the framework of classical chemical kinetics, the phenomenon is illustrated with the minimal M ⇌ I ⇌ N scheme. From the denaturant dependencies of the microscopic rate constants, calculated by diagonalizing the rate matrix, the rate constants in water (inverse seconds) and $m^{\ddagger}$ values (kilocalories per mole per molar) for the four processes are as follows: $k^{\circ}_{MI} = 1 \times 10^6$, $m^{\ddagger}_{MI} = -0.5$, $k^{\circ}_{IM} = 500$, $m^{\ddagger}_{IM} = 0.5$, $k^{\circ}_{IN} = 1.24 \times 10^5$, $m^{\ddagger}_{IN} = -0.037$, $k^{\circ}_{NI} = 10$, and $m^{\ddagger}_{NI} = 0.037$. (B) Dependence of the amplitude of the microsecond relaxation process fits to the equilibrium unfolding transition of CO-liganded ferrocyt *c* (ΔG°=10.34 kcal mol^{-1}, and m_g=2.92 kcal mol^{-1} M^{-1}. This analysis would appear inconsistent, from the viewpoint of traditional analysis, with transient trapping of the intermediate I (but see the text).

local tertiary conformational changes following laser photolysis of carbonmonoxyhemoglobin (*50*).

Rate Rollover and Accumulation of Kinetic Intermediates. The thermodynamically distinct molten globule-like nature of the M state facilitates analysis of the rate−stability data within the formalism of a folding chevron. The rate rollover under strongly nativelike conditions is a distinctive feature of the chevron plot for the M → N transition (Figure 3a). Rollover to varying extents has been observed for numerous proteins, as illustrated in Figure 1b for ferrocyt *c* and carbonmonoxycyt *c*, although the refolding limb of nitrosylcyt *c* does not exhibit this phenomenon (*36*). Unfortunately, a clear understanding of curvatures in the plot of the logarithm of folding rates versus denaturant concentration is lacking. A number of factors, individually or in combination, may be associated with rollover in a case specific manner. In the funnel paradigm, a protein whose energy landscape in the absence of denaturant is sufficiently smooth should not exhibit a rollover, as observed for nitrosylcyt *c* (*36*), CspB (*51*), and CI2 (*52*). Analyses of coarse-grained protein chain models indicate that rollover may result from an internal frictional effect that impedes chain motions under strongly nativelike conditions (*53*−*55*). Using the principles of classical kinetics, the rollover has been explained by invoking the accumulation of at least one structural intermediate whose slower rate of folding limits the observed folding rate (*56*). Yet another possible cause for rollover is a broad energy barrier that separates the native state from the initial state. The rate-limiting transition-state ensemble which is the highest point on the barrier energy profile moves toward the unfolded state when nativelike conditions are approached, giving rise to rate rollover in the refolding limb of the chevron. This model was used to explain chevron curvature for the two-state protein U1A (*57*). Indeed, these subtly different explanations convey the same general picture that folding decelerates because of roughness toward the bottom of the funnel. A contribution to the roughness may come from one or more stable intermediates as exemplified by extensive native-state hydrogen exchange data on ferricyt *c* (*27*, *29*), kinetic traps set up by non-native interactions that may originate from nonspecific collapse of the initial unfolded state or from proline isomerization, and internal frictional effects that are intensified by frustrating interactions causing the traps to deepen. From this synthesis, we attribute the accentuated rollover in the folding chevron of the M → N transition to at least one kinetic trap, the structural nature and the causative interactions of which stand to scrutiny. In phenomenological terms, the minimalist scheme is then M ⇌ I ⇌ N, where I is a trapped intermediate that occupies an energy well. The microscopic rate constants shown in Figure 3a represent one of the eigenvalue solutions of the kinetic model. At higher denaturant concentrations where the intermediate is destabilized, the denaturant function of the observed rate is linear, and the rate constant measured is that for the two-state M → N transition, k_{MN}. Linear extrapolation of k_{MN} values to the ordinate provides the fastest rate for the folding of ferrocytochrome *c*. The phenomenological three-state nature of the M → N transition becomes visible only when the glassy trap deepens under strongly nativelike conditions reflected by the chevron rollover.

The amplitude of the single-phase microsecond spectral change as a function of GdnHCl is shown in Figure 3b. In this time regime, we do not observe denaturant-dependent missing amplitude. Any ultrafast signal decay, which is beyond the resolution of our spectrometer, can be attributed to heme-associated electronic structural changes immediately after photodissociation of CO. The denaturant-dependent changes in the observed amplitude (Figure 3b) are as expected from the observed mass action effect of CO on the unfolding transition of ferrocyt *c* (Figure 2c). The denaturant−amplitude data best fit a two-state M → N transition (Figure 3b), the iterated fit parameters for which are within 12% of the values obtained from independently measured data. Clearly, this is not a fit to the M ⇌ I ⇌ N model, nor is it consistent with the missing amplitude analysis for accumulation of intermediates (*56*, *58*). The observation of chevron rollover with no missing amplitude might appear to make the existence of I doubtful. While the rollover in the rate-denaturant data suggests the intermediate state, the denaturant distribution of the decay amplitude does not. However, the visible optical probe employed here (550 nm) may be silent to a possible tertiary structural change associated with the formation of I that leads the M80 ligation event. An illustration of this point is found in the recent "downhill folding" experiments with the λ_{6-85} protein (*26*). Also, spectra of deligated or five-coordinate hemes could be quite complex (*59*), and optical changes as a result of local tertiary structural adjustments in the photoproduct are not assured. Further, missing amplitude is not a necessary and sufficient criterion for chevron rollover. Simple single-exponential folding kinetics, which become increasingly insensitive to denaturant as strongly nativelike conditions are approached, can often produce rate rollover and reveal kinetic

trapping and glassy dynamics (*53*). The data presented in panels a and b of Figure 3 are consistent with this interpretation of the folding transition.

Although the data available at this point are not quite adequate to provide mechanistic insights into the M → N transition, a simple model may be contemplated on the basis of what is expected to happen in the photoproduct. As established by a number of seminal photodissociation studies of CO-bound heme proteins (*60*−*64*), protein tertiary conformational changes emerge only in nanoseconds or longer. This time is well within the range expected for local structural organization (*45*), or for fast folding of short loops, helices, and side chains (*33*, *65*). The time range of ∼10−500 ns has been associated with an adjustment of the local tertiary structure into the void created by the departing CO ligand in hemoglobin (*50*). It is likely that such a structural rearrangement that is perhaps spectrally silent occurs in the photolyzed product of the M state, leading to transient accumulation of the species labeled I. Further folding involves the native-state M80 ligation to the heme iron and is limited by reorganization of presumably misfolded side chain elements to facilitate the formation of a contact between Fe^{2+} and the sulfur of M80. This speculative model must be treated cautiously before a more complete picture of postphotolysis dynamics is obtained.

The Reverse Sodium Sulfate Effect for I → N Folding Suggests that I Is a Trapped Misfolded Intermediate. To understand the nature of the tertiary interactions in I, we measured the folding rate as a function of the stabilizing salt, Na_2SO_4. The rationale was that Na_2SO_4, which is known to stabilize intermediate species (*66*), would retard the rate of I → N conversion if I contained tertiary interactions that were not nativelike. In a folding scenario in which the interactions become increasingly nativelike (Q) as the protein runs down the funnel, Na_2SO_4 will stabilize a transition state with a higher Q value more than a state that is less compact. Consequently, the rate will increase with an increase in the Na_2SO_4 concentration. As Figure 4a shows, at a constant GdnHCl concentration (0.3 M), the measured I → N folding rate decreases monotonously with an increase in the concentration of Na_2SO_4, suggesting that the transition state (TS) for the I → N segment exposes more surface area than the I state. The addition of sulfate stabilizes the I state with respect to the TS because I is the more compact state, the consequence being a decrease in the observed folding rate. By this explanation, to achieve the correct conformation with respect to the N state, an unfolding event that would disperse the incorrect organization in the I state is necessary. Accordingly, the intermediate could be regarded as a trapped misfolded structure, a prototype of dynamically frozen late intermediates predicted by the funnel theory (*11*). The emerging picture then is that in response to the exit of the photolyzed CO ligand, the tertiary structure of the M state configures nonspecifically to give rise to the I state. One or more interactions in I are geometrically and (or) energetically frustrated; they act as kinetic traps, and the rate of their reorganization into the correct state limits the formation of the native Fe^{2+}−M80 bond.

Fairly Sizable Energy Barrier for I → N Folding. To estimate the energy scale for the interactions that must be reconfigured to establish the N state, we looked at the temperature dependence of I → N folding (Figure 4b).

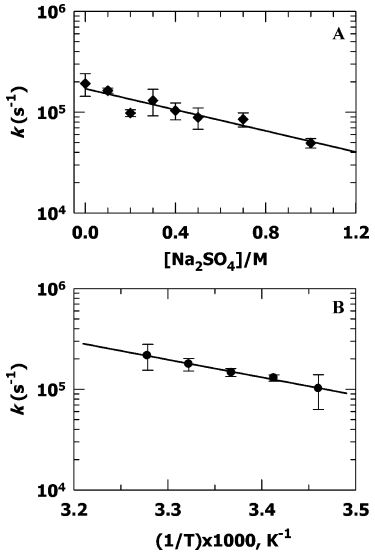

FIGURE 4: (A) Monotony of the decrease in the I → N folding rate with increments of Na_2SO_4 in the folding milieu which suggests that I is indeed misfolded. The transition state from I to N thus exposes relatively more surface area, with the consequence that it is stabilized less by sulfate. (B) Barrier for the I → N transition is substantial ($E_a = 8 \pm 1$ kcal/mol), consistent with the observation that the transition state is weakly stabilized by sulfate.

Assuming the applicability of the thermally activated rate law, the derived activation energy $E_a = 8 \pm 1$ kcal/mol and the prefactor $A_o \sim 1.2 \times 10^{11}$ s^{-1}. Such a strong temperature dependence is conceivable at very late stages of folding where intrachain reorganizations of the kind pondered here are necessary. The conformational energy difference between I and N is just approximately a few k_BT; I is less mobile and is as compact as N, implying no significant enthalpic and entropic mismatch in I. The observed barrier energy then is likely to originate from substantial reorganization of nonnative interactions in I. The TS is thus relatively more unfolded, little stabilized by sulfate, and is sizable in energy. Similar strong thermal activation and a large Arrhenius prefactor have been reported for α-helix formation in a photoswitchable peptide that displays stretched exponential, and the authors relate the observed thermal activation to multiple local barriers between misfolded microstates or, equivalently, to activated diffusion on a rugged energy landscape (*33*).

Glassy Folding of the M State of Ferrocyt c. The conclusions reached here are consistent with at least two earlier studies. Theoretical studies of Chan and co-workers (*53*, *54*, *67*) show that rollover in the folding chevron may often be a consequence of kinetic traps, and hence glassy dynamics under nativelike conditions. The role of internal friction effect under nativelike conditions is also documented by the experiments of Hagen and co-workers (*39*). While the results of this study agree with theirs, it is also shown here that chain misconfiguration at very late stages of folding intensifies the frictional effects producing rate rollovers and glassy dynamics for cytochrome *c*. Misconfiguration and the consequent geometric frustration deepen the energy minima and obviously produce more drag forces. Kinetic traps and internal friction are related phenomena. Internal friction could be considered a kinetic trap because it decelerates folding, but kinetic traps are more direct manifests of chain misorganization. They make the landscape rugged because energy

barriers to chain reorganization giving rise to drag forces exist. It is interesting to note that varying degrees of internal friction persist at all stages of folding. Even the native state experiences internal friction, because the protein structure in solution is dynamic. Thus, a perfectly smooth folding funnel should not exist. The energy landscape theory does find that the folding funnel is generally rugged toward the bottom where molten globule-like states have already crossed over the glass transition-state region (*1*, *3*, *11*). In a highly rugged funnel where the minima are deeper than a few k_BT, folding becomes glassy and decelerates because of transient trapping of structures in the local minima. Folding of these structures containing non-native interactions will be dominated by the rate of their exit from the kinetic traps. The data for the folding of the molten globule-like M state corroborate these predictions, although we still do not have complete information about the structural changes involved in the M → I transition. The frustrated interactions that trap the I-like microstates and whose reorganization limits the folding within this segment of the folding coordinate remain to be investigated. Finally, the overall folding rate of a protein could be limited by such late glass transitions only if the earlier folding events are faster than the rate of exit from the glassy traps.

SUPPORTING INFORMATION AVAILABLE

Basic spectral data, including one-dimensional proton NMR spectra, for the NCO or M state. This material is available free of charge via the Internet at http://pubs.acs.org.

REFERENCES

1. Bryngelson, J. D., and Wolynes, P. G. (1987) Spin-glasses and the statistical mechanics of protein folding, *Proc. Natl. Acad. Sci. U.S.A. 84*, 7524−7528.
2. Onuchic, J. N., Wolynes, P. G., Luthey-Schulten, Z., and Socci, N. D. (1995) Toward an outline of the topography of a realistic protein-folding funnel, *Proc. Natl. Acad. Sci. U.S.A. 92*, 3626−3630.
3. Bryngelson, J. D., Onuchic, J. N., Socci, N. D., and Wolynes, P. G. (1995) Funnels, pathways and the energy landscape of protein folding: A synthesis, *Proteins 21*, 167−195.
4. Thirumalai, D., Ashwin, V., and Bhattacharjee, J. K. (1996) Dynamics of random hydrophobic-hydrophilic copolymers, *Phys. Rev. Lett. 77*, 5385−5388.
5. Dill, K. A., and Chan, H. S. (1997) From Levinthal to pathways to funnels, *Nat. Struct. Biol. 4*, 10−19.
6. Nymeyer, H., Garcia, A. E., and Onuchic, J. N. (1998) Folding funnels and frustration in off-lattice minimalist protein landscapes, *Proc. Natl. Acad. Sci. U.S.A. 95*, 5921−5928.
7. Socci, N. D., Onuchic, J. N., and Wolynes, P. G. (1998) Protein folding mechanisms and the multidimensional folding funnel, *Proteins 32*, 136−158.
8. Schonbrun, J., and Dill, K. A. (2003) Fast protein folding kinetics, *Proc. Natl. Acad. Sci. U.S.A. 100*, 12678−12682.
9. Onuchic, J. N., and Wolynes, P. G. (2004) Theory of protein folding, *Curr. Opin. Struct. Biol. 14*, 70−75.
10. Wolynes, P. G. (2005) Energy landscapes and solved protein-folding problems, *Philos. Trans. R. Soc. London, Ser. A 363*, 453−467.
11. Wolynes, P. G., Onuchic, J. N., and Thirumalai, D. (1995) Navigating the folding routes, *Science 267*, 1619−1620.
12. Lazaridis, T., and Karplus, M. (1997) "New view" of protein folding reconciled with the old through multiple unfolding simulations, *Science 278*, 1928−1931.
13. Dobson, C. M., Sali, A., and Karplus, M. (1998) Protein folding: A perspective from theory and experiments, *Angew. Chem., Int. Ed. 37*, 868−893.
14. Nymeyer, H., Socci, N. D., and Onuchic, J. N. (2000) Landscape approaches for determining the ensemble of folding transition states: Success and failure hinge on the degree of frustration, *Proc. Natl. Acad. Sci. U.S.A. 97*, 634−639.
15. Clementi, C., Jennings, P. A., and Onuchic, J. N. (2000) How native-state topology affects the folding of dihydrofolate reductase and interleukin-β, *Proc. Natl. Acad. Sci. U.S.A. 97*, 5871−5876.
16. Koga, N., and Takada, S. (2001) Roles of native topology and chain-length scaling in protein folding: A simulation study with a Go-like model, *J. Mol. Biol. 313*, 171−180.
17. Garcia, A. E., and Onuchic, J. N. (2003) Folding a protein in a computer: An atomic description of the folding/unfolding of protein A, *Proc. Natl. Acad. Sci. U.S.A. 100*, 13898−13903.
18. Pogorelov, T. V., and Luthey-Shulten, Z. (2004) Variations in the fast folding rates of the λ-repressor: A hybrid molecular dynamics study, *Biophys. J. 87*, 207−214.
19. Jones, C. M., Henry, E. R., Hu, Y., Chan, C. K., Luck, S., Bhuyan, A., Roder, H., Hofrichter, J., and Eaton, W. A. (1993) Fast events in protein folding initiated by nanosecond laser photolysis, *Proc. Natl. Acad. Sci. U.S.A. 90*, 11860−11864.
20. Williams, S., Causgrove, T. P., Gilmanshin, R., Fang, K. S., Callender, R. H., Woodruff, W. H., and Dyer, R. B. (1996) Fast events in protein folding: Helix melting and formation in a small peptide, *Biochemistry 35*, 691−697.
21. Goldbeck, R. A., Thomas, Y. G., Chen, E., Esquerra, R. M., and Kliger, D. S. (1999) Multiple pathways on a protein-folding energy landscape: Kinetic evidence, *Proc. Natl. Acad. Sci. U.S.A. 96*, 2782−2787.
22. Snow, C. D., Nguyen, N., Pande, V. S., and Gruebele, M. (2002) Absolute comparison of simulated and experimental protein-folding dynamics, *Nature 420*, 102−106.
23. Matouschek, A., Kellis, J. T., Serrano, L., and Fersht, A. R. (1989) Mapping the transition state and pathway of protein folding by protein engineering, *Nature 340*, 122−126.
24. Fersht, A. R. (1997) Nucleation mechanism in protein folding, *Curr. Opin. Struct. Biol. 7*, 3−9.
25. Zong, C., Wilson, C. J., Shen, T., Wolynes, P. G., and Wittung-Stafshede, P. (2006) ϕ-Value analysis of apo-azurin folding: Comparison between experiment and theory, *Biochemistry 45*, 6458−6466.
26. Ma, H., and Gruebele, M. (2005) Kinetics are probe-dependent during downhill folding of an engineered λ_{6-85} protein, *Proc. Natl. Acad. Sci. U.S.A. 102*, 2283−2287.
27. Bai, Y., Sosnick, T. R., Mayne, L., and Englander, S. W. (1995) Protein folding intermediates: Native-state hydrogen exchange, *Science 269*, 192−197.
28. Englander, S. W., Sosnick, T. R., Mayne, L. C., Shtilerman, M., Qi, P. X., and Bai, Y. (1998) Fast and slow folding in cytochrome c, *Acc. Chem. Res. 31*, 737−744.
29. Hoang, L., Bédard, S., Krishna, M. M. G., Lin, Y., and Englander, S. W. (2002) Cytochrome c folding pathway: Kinetic native-state hydrogen exchange, *Proc. Natl. Acad. Sci. U.S.A. 99*, 12173−12178.
30. Angell, C. A. (1995) Formation of glasses from liquids and biopolymers, *Science 267*, 1924−1935.
31. Morozova-Roche, L. A., Jones, J. A., Noppe, W., and Dobson, C. M. (1999) Independent nucleation and heterogeneous assembly of structure during folding of equine lysozyme, *J. Mol. Biol. 289*, 1055−1073.
32. Leeson, D. T., Gai, F., Rodrigues, H. M., Gregoret, L. M., and Dyer, R. B. (2000) Protein folding and unfolding on a complex energy landscape, *Proc. Natl. Acad. Sci. U.S.A. 97*, 2527−2532.
33. Bredenbeck, J., Helbing, J., Kumita, J. R., Wooley, G. A., and Hamm, P. (2005) α-Helix formation in a photoswitchable peptide tracked from picoseconds to microseconds by IR spectroscopy, *Proc. Natl. Acad. Sci. U.S.A. 102*, 2379−2384.
34. Gillespie, B., and Plaxco, K. W. (2000) Nonglassy kinetics in the folding of a simple single-domain protein, *Proc. Natl. Acad. Sci. U.S.A. 97*, 12014−12019.
35. Bhuyan, A. K., and Kumar, R. (2002) Kinetic barriers to the folding of horse cytochrome c in the reduced state, *Biochemistry 41*, 12821−12834.
36. Prabhu, N. P., Kumar, R., and Bhuyan, A. K. (2004) Folding barrier in horse cytochrome c: Support for a classical folding pathway, *J. Mol. Biol. 337*, 195−208.
37. Bhuyan, A. K. (2002) Protein stabilization by urea and guanidine hydrochloride, *Biochemistry 41*, 13386−13394.
38. Kumar, R., Prabhu, N. P., Yadaiah, M., and Bhuyan, A. K. (2004) Protein stiffening and entropic stabilization in the subdenaturing limit of guanidine hydrochloride, *Biophys. J. 87*, 2656−2662.

39. Pabit, S. A., Roder, H., and Hagen, S. J. (2004) Internal friction controls the speed of protein folding from a compact configuration, *Biochemistry 43*, 12532−12538.
40. Ptitsyn, O. B. (1995) Molten globule and protein folding, *Adv. Protein Chem. 47*, 83−229.
41. Rao, D. K., Kumar, R., Yadaiah, M., and Bhuyan, A. K. (2006) The alkali molten globule state of ferrocytochrome c: Extraordinary stability, persistent structure, and constrained overall dynamics, *Biochemistry 45*, 3412−3420.
42. Hagen, S. J., Carswell, C. W., and Sjolander, E. W. (2001) Rate of intrachain contact formation in an unfolded protein: Temperature and denaturant effects, *J. Mol. Biol. 305*, 1161−1171.
43. Hagen, S. J., Latypov, R. F., Dolgikh, D. A., and Roder, H. (2002) Rapid intrachain binding of histidine-26 and histidine-33 to heme in unfolded ferrocytochrome *c*, *Biochemistry 41*, 1372−1380.
44. Kumar, R., Prabhu, N. P., and Bhuyan, A. K. (2005) Ultrafast events in the folding of ferrocytochrome *c*, *Biochemistry 44*, 9359−9367.
45. Ballew, R. M., Sabelko, J., and Gruebele, M. (1996) Observation of distinct nanosecond and microsecond protein folding events, *Nat. Struct. Biol. 3*, 923−926.
46. Hammes, G. G., and Roberts, P. B. (1969) Dynamics of the helix-coil transition in poly-L-ornithine, *J. Am. Chem. Soc. 91*, 1812−1816.
47. Thompson, P. A., Eaton, W. A., and Hofrichter, J. (1997) Laser temperature jump study of the helix-coil kinetics of an alanine peptide interpreted with a 'kinetic zipper' model, *Biochemistry 36*, 9200−9210.
48. Lednev, I. K., Karnoup, A. S., Sparrow, M. C., and Asher, S. A. (1999) α-Helix peptide folding and unfolding activation barriers: A nanosecond UV resonance Raman study, *J. Am. Chem. Soc. 121*, 8074−8086.
49. Eaton, W. A., Muñoz, V., Thompson, P. A., Henry, E. R., and Hofrichter, J. (1998) Kinetics and dynamics of loops, α-helices, *β*-hairpins, and fast-folding proteins, *Acc. Chem. Res. 31*, 745−753.
50. Murray, L. P., Hofrichter, J., Henry, E. R., and Eaton, W. A. (1988) Time-resolved optical spectroscopy and structural dynamics following photodissociation of carbonmonoxyhemoglobin, *Biophys. Chem. 29*, 63−76.
51. Schindler, T., Herrler, M., Marahiel, M. A., and Schmid, F. X. (1995) Extremely rapid protein folding in the absence of intermediates, *Nat. Struct. Biol. 2*, 663−673.
52. Jackson, S. E., and Fersht, A. R. (1991) Folding of chymotrypsin inhibitor-2. 1. Evidence for a two-state transition, *Biochemistry 30*, 10428−10435.
53. Kaya, H., and Chan, H. S. (2002) Towards a consistent modeling of protein thermodynamics and kinetic cooperativity: How applicable is the transition state picture to folding and unfolding, *J. Mol. Biol. 315*, 899−909.
54. Kaya, H., and Chan, H. S. (2002) Solvation effects and driving forces for protein thermodynamic and kinetic cooperativity: How adequate is native-centric topological modeling, *J. Mol. Biol. 326*, 911−931.
55. Chan, H. S., Shimizu, S., and Kaya, H. (2004) Cooperativity principles in protein folding, *Methods Enzymol. 380*, 350−379.
56. Khorasanizadeh, S., Peters, I. D., and Roder, H. (1996) Evidence for a three-state model of protein folding from kinetic analysis of ubiquitin variants with alterd core residues, *Nat. Struct. Biol. 3*, 193−205.
57. Otzen, D. E., Kristensen, O., Proctor, M., and Oliveberg, M. (1999) Structural changes in the transition state of protein folding: Alternative interpretations of curved chevron plots, *Biochemistry 38*, 6499−6511.
58. Ikeguchi, M., Kuwajima, K., Mitani, M., and Sugai, S. (1986) Evidence for identity between the equilibrium unfolding intermediate and a transient folding intermediate: A comparative study of the folding reactions of α-lactalbumin and lysozyme, *Biochemistry 25*, 6965−6972.
59. Eaton, W. A., and Hofrichter, J. (1981) Polarized absorption and linear dichroism spectroscopy of hemoglobin, *Methods Enzymol. 76*, 175−261.
60. Greene, B. I., Hochstrasser, R. M., Weisman, R. B., and Eaton, W. A. (1978) Spectroscopic studies of oxy- and carbonmonoxy-hemoglobin after pulsed optical excitation, *Proc. Natl. Acad. Sci. U.S.A. 75*, 5255−5259.
61. Chernoff, D. A., Hochstrasser, R. M., and Steele, A. W. (1980) Geminate recombination of O_2 and hemoglobin, *Proc. Natl. Acad. Sci. U.S.A. 77*, 5606−5610.
62. Terner, J., Stong, J. D., Spiro, T. G., Nagumo, M., Nicol, M., and El-Sayed, M. A. (1981) Picosecond resonance Raman spectroscopic evidence for excited-state spin conversion in carbonmonoxy-hemoglobin photolysis, *Proc. Natl. Acad. Sci. U.S.A. 78*, 1313−1317.
63. Terner, J., Spiro, T. G., Nagumo, M., Nicol, M. F., and El-Sayed, M. A. (1980) Resonance Raman spectroscopy in the picosecond time scale: The carbonmonoxy photointermdeiate, *J. Am. Chem. Soc. 102*, 3238−3239.
64. Findsen, E. W., Friedman, J. M., Ondrias, M. R., and Simon, S. R. (1985) Picosecond time-resolved resonance Raman studies of hemoglobin: Implications for reactivity, *Science 229*, 661−665.
65. Krieger, F., Fierz, B., Bieri, O., Drewello, M., and Kiefhaber, T. (2003) Dynamics of unfolded polypeptide chains as model for the earliest steps in protein folding, *J. Mol. Biol. 332*, 265−274.
66. von Hippel, P. H., and Wong, K.-Y. (1965) On the conformational stability of globular proteins. The effect of various electrolytes and nonelectrolytes on the thermal ribonuclease transition, *J. Biol. Chem. 240*, 3909−3923.
67. Portman, J. J., Takada, S., and Wolynes, P. G. (2001) Microscopic theory of protein folding rates. II. Local reaction coordinate and chain dynamics, *J. Chem. Phys. 114*, 5082−5096.

BI062193U